JOURNAL OF THERMOPHYSICS AND HEAT TRANSFER
Vol. 8, No. 4, Oct.–Dec. 1994

Thermochemical Nonequilibrium Viscous Shock-Layer Analysis for a Mars Aerocapture Vehicle

Kojiro Suzuki* and Takashi Abe†
Institute for Space and Astronautical Science, Sagamihara, Kanagawa 229, Japan

The effects of thermal and chemical nonequilibrium on the aerothermodynamic environment over a Mars aerocapture vehicle are studied. In order to understand the characteristics of the flow at aerobraking, the classification of the stagnation region flow has been carried out from a viewpoint of the extent of the thermal and chemical nonequilibrium in the shock layer. The numerical analysis of the forebody flowfield over a spacecraft has been made by using the viscous shock-layer equations, including the thermal and chemical nonequilibrium effects of carbon dioxide. The influences of the thermal nonequilibrium on the flow properties in the shock layer become significant at an altitude above 60 km. As for the wall heating rate, however, its influence is not as strong as the influence of the wall catalycity. The sensitivities of the wall heating rate to the uncertainties in the real gas effect models are investigated parametrically. The wall heating rate is strongly affected by the wall catalycity. Consequently, a chemical nonequilibrium flow analysis is necessary for the analysis of the aerothermodynamic environment of a Mars aerocapture vehicle.

Nomenclature

C_i = mass fraction of ith species
$C_{p,i}$ = specific heat at constant pressure of ith species
$C_{v,i}$ = specific heat at constant volume of ith species
$e_{v,i}$ = vibrational energy of ith species per unit mass
h_i = enthalpy of ith species
$h_{0,i}$ = heat of formation of ith species
k_f = forward reaction rate coefficient
k_i = thermal conductivity of ith species
L = characteristic length for relaxation process
M_i = molecular weight of ith species
$Q_{V,i}$ = rate of energy transfer due to vibrational relaxation for ith species
R_N = nose radius
s = coordinate measured from apex along the body surface
T_{ref} = reference temperature for heat of formation
u = velocity component in x direction
W_i = mass rate of production of ith species per unit volume
x = distance measured from the shock wave
y = coordinate normal to the body surface
Z_i = third body efficiency of ith species
Δf = nonequilibrium quantity behind the shock wave
δ = shock standoff distance
$\theta_{V,i}$ = characteristic temperature of vibrational energy mode for ith species
μ_i = viscosity of ith species
ρ_i = density of ith species
$\langle \tau_i \rangle$ = effective vibrational relaxation time for ith species

Subscripts
chem = chemical relaxation process
r = rotational energy mode of molecule
shock = value just behind the shock wave
T-V = translational-vibrational energy relaxation
t = translational energy mode of molecule
v = vibrational energy mode of molecule
wall = wall value

Superscripts
eq = value at equilibrium state
ref = value at reference state

Introduction

FOR a mission to a planet with an atmosphere, the aerobraking technique is known to be useful in order to augment the payload capability of the spacecraft.[1] It enables one to save the spacecraft fuel required for orbital maneuvering by utilizing aerodynamic drag during the atmospheric flight. An in-house feasibility study of a Mars exploration mission using the aerobraking technique[2] showed that this technique can be implemented successfully. It ensures the increase in the scientific payload mass within the total spacecraft mass that is restricted due to the capability of the launch vehicle.

The influences of the thermal and chemical nonequilibrium of the flow on the aerothermodynamic environment around a vehicle at the Mars aerobraking should be clarified by numerical analysis of the thermal and chemical nonequilibrium flow over a spacecraft. All the real gas effects required for the analysis of the aerothermodynamic environment around an aerocapture vehicle should be described appropriately by a mathematical modeling with some parameters. Most of them, however, include many unknown factors that can hardly be specified. For instance, we have a rough model for the wall catalycity that has a significant effect on the aerodynamic heating rate.[3,4] The two limiting conditions with respect to the wall catalycity, i.e., the non-catalytic wall (NCW) and the fully catalytic wall (FCW) conditions, are known to be appropriate in order to determine the lower and the upper limits of the heating rate, respectively. From a viewpoint of the design of the spacecraft, it is important to know the sensitivities of the aerothermodynamic environment to the uncertainties in the real gas effect models by making parametric studies.

In the present study, the hypersonic axisymmetric forebody flowfield over a spacecraft at the Mars aerobraking is studied numerically by using the viscous shock-layer equations that include the chemical reaction effects[5] and the thermal non-

Presented as Paper 93-2839 at the AIAA 28th Thermophysics Conference, Orlando, FL, July 6–9, 1993; received Jan. 7, 1994; revision received May 16, 1994; accepted for publication May 20, 1994.

*Research Associate, Research Division for Space Transportation, 3-1-1 Yoshinodai. Member AIAA.
†Professor, Research Division for Space Transportation, 3-1-1 Yoshinodai. Member AIAA.

equilibrium effects. The chemical species considered are CO_2, CO, C, O, C_2, O_2, CO^+, and e^-. The two-temperature model by Park[6] is employed for the thermochemical nonequilibrium analysis.

The major objectives in the present study are 1) to make a classification of the stagnation region flow chemistry for a Mars aerocapture vehicle, 2) to investigate the effects of the thermal and chemical nonequilibrium on the aerothermodynamic environment around a spacecraft at the Mars aerobraking, and 3) to investigate the sensitivities of the aerothermodynamic environment around a spacecraft to the uncertainties in the modeling of the real gas effects of carbon dioxide.

Method of Analysis

In this section, we present a simple method to classify the stagnation region flow chemistry for a Mars aerocapture vehicle. After that, the physical model of reacting carbon dioxide for the thermal and chemical nonequilibrium viscous shock-layer analysis is discussed.

Martian Atmosphere Model and Vehicle Configuration

To make classification of the stagnation region flow chemistry, the physical properties of the Martian atmosphere and the vehicle size must be specified. The atmospheric density determines the rate of the molecular collisions and affects the extent of the flow nonequilibrium. In the present study, the "most probable" model in Ref. 7 is used. It should be noted that there are many uncertainties in the physical properties of the Martian atmosphere. In fact, the atmospheric density of the most probable model is two or three times higher than that determined from the flight data of the Viking 1 and 2 spacecrafts,[8] at an altitude of around 50 km. The Martian atmosphere is known to be composed of CO_2 and N_2. But in the present study, only CO_2 is considered as the freestream composition, since the mass fraction of N_2 is small.

On the other hand, the nose radius also affects the extent of the flow nonequilibrium in the shock layer in the stagnation region, since it determines the transit time of molecules in this region. In the present study, we consider a spherically blunted cone having a diameter of 2.4 m at the base, a cone angle of 120 deg, and a nose radius of 1 m as a typical vehicle configuration for the Mars aerocapture. The entry velocity to the Martian atmosphere and the perigee altitude are considered to be around 6 km/s and 40 km as a nominal case for this configuration, respectively. Since our interests are mainly focused on the aerothermodynamic environment of the aerocapture vehicle at the flight regime of a severe wall heating rate, the flight velocity is nominally fixed as 6 km/s.

Classification of Flow Chemistry

For both the chemical and thermal nonequilibrium, we assume the relaxation process in which the nonequilibrium quantities generated initially just behind the normal shock wave vanish asymptotically with the increase in the distance from the shock wave. The length scale for the shock-layer flow is evaluated by the shock standoff distance. Then the value of Δf_δ defined by

$$\Delta f_\delta = \Delta f_{\text{shock}} \cdot \exp(-\delta/L) \tag{1}$$

represents the magnitude of the flow nonequilibrium in the shock layer. When the value of Δf_δ becomes large, the shock layer is expected to be more significantly affected by the flow nonequilibrium. In the above expression, both the magnitude of the flow nonequilibrium generated just behind the shock wave and its relaxation rate in the shock layer are taken into account. In the present study, δ is assumed to be 10% of the nose radius. The definition of the nonequilibrium quantity and the method to determine the characteristic length for the chemical nonequilibrium and the thermal nonequilibrium are given in the following.

For the evaluation of the extent of the chemical nonequilibrium, only the dissociation reaction of carbon dioxide

$$CO_2 + M \leftrightarrow CO + O + M \qquad (M = CO_2, CO, O) \tag{2}$$

is considered, since it is the primary reaction in the shock layer of a Mars aerocapture vehicle.[5] The flow is assumed to be in the thermal equilibrium. The mass fraction of CO_2, which is 100% just behind the shock wave in the frozen chemistry, is assumed to relax toward the value determined by the shock relations with the equilibrium chemistry. Then the nonequilibrium quantity for the chemical relaxation is defined as the deviation of the mass fraction of CO_2 from its chemical equilibrium value behind the shock wave as follows:

$$\Delta f = C_{CO_2} - C^{\text{eq}}_{CO_2} \tag{3}$$

The steady-state species continuity equation for CO_2 is given as

$$\frac{\partial(\rho_{CO_2} \cdot u)}{\partial x} = W_{CO_2} \tag{4}$$

Equation (4) can be linearized with respect to Δf as follows:

$$u^{\text{ref}} \frac{d\Delta f}{dx} = -k_f^{\text{ref}} \rho^{\text{ref}} \left(\sum_i Z_i \cdot \frac{C_i}{M_i} \right)^{\text{ref}} \cdot \Delta f \qquad (i = CO_2, CO, O) \tag{5}$$

The reference values required for the linearization are determined by taking an average of the conditions just behind the shock wave with the frozen chemistry and those with the equilibrium chemistry. The conditions behind the shock wave are computed by the Rankine-Hugoniot relations. Then the characteristic length for the relaxation of the chemical nonequilibrium is determined as follows:

$$L_{\text{chem}} = \frac{|u^{\text{ref}}|}{k_f^{\text{ref}} \rho^{\text{ref}} \left(\sum_i Z_i \cdot \frac{C_i}{M_i} \right)^{\text{ref}}} \qquad (i = CO_2, CO, O) \tag{6}$$

As for the thermal nonequilibrium, the chemical reactions are assumed to be frozen at the freestream composition, and the relaxation process between the translational energy mode and the vibrational energy mode (T-V relaxation) of CO_2 is considered. The difference between the translational temperature and the vibrational temperature is considered as the nonequilibrium quantity for the thermal nonequilibrium. The characteristic length for the T-V relaxation is determined by using the effective vibrational relaxation time for CO_2 as follows:

$$L_{T\text{-}V} = |u^{\text{ref}}| \cdot \langle \tau_{CO_2} \rangle^{\text{ref}} \tag{7}$$

In the thermal nonequilibrium case, the reference values are determined by taking an average of the conditions behind the shock wave with the thermally frozen state and those with the thermal equilibrium state.

Nonequilibrium Viscous Shock-Layer Analysis

To investigate the thermal and chemical nonequilibrium effects on the aerothermodynamic environment for a Mars aerocapture vehicle, two kinds of analyses have been carried out. One is the viscous shock-layer analysis with the nonequilibrium chemistry of CO_2 under the assumption of the thermal equilibrium, and the other is the viscous shock-layer analysis including both the chemical nonequilibrium and the

thermal nonequilibrium. By comparisons between the results by the above two kinds of analyses, we can assess the importance of the effect of the thermal nonequilibrium on the aerothermodynamic environment around a spacecraft at the Mars aerobraking. The details of the models used for the present study are given in Ref. 9.

Chemical Nonequilibrium Analysis

The axisymmetric viscous shock-layer equations with the nonequilibrium chemistry that is composed of eight species, i.e., CO_2, CO, C, O, C_2, O_2, CO^+, and e^-, are solved. All the reactions considered in the present study and their reaction rates are taken from the work by Blottner.[10] The radiation in the shock layer is not considered, since the radiative heating is not significant at the entry velocity of 6 km/s.[11] The flow is assumed to be laminar, since the freestream Reynolds number referred to the nose radius does not exceed 10^6, even at the perigee altitude. The governing equations for the present study are basically the same as those for the air that are given in detail in Refs. 12 and 13. The models used to describe the real gas effects of carbon dioxide are explained briefly in the following.

The specific heat and enthalpy for the eight-species CO_2 model are computed from the polynomial curve fits in terms of the temperature up to 30,000 K, which is high enough for the study of the shock layer of a Mars aerocapture vehicle. The curve-fits have been performed to the results of the specific heat computed from the spectroscopic data by Allison's method.[14]

The viscosity of each species is given by the logarithmic curve-fit in terms of the temperature.[10] The thermal conductivity of each species is expressed as the summation of the translational, rotational, and vibrational components as follows:

$$\begin{aligned} k_i &= k_{t,i} + k_{r,i} + k_{V,i} \\ k_{t,i} &= \mu_i \cdot \tfrac{5}{2} C_{Vt,i} \\ k_{r,i} &= \tfrac{6}{5} \mu_i \cdot C_{Vr,i} \\ k_{V,i} &= k_{r,i} \end{aligned} \tag{8}$$

which are derived from Eucken's relation.[15] The viscosity and the thermal conductivity of the gas mixture are evaluated by Wilke's semiempirical method.[12] The diffusion phenomena of the gas species are described by the binary diffusion model.[6] The diffusion mass flux is considered only in the normal direction to the wall. The diffusion coefficient is computed by assuming a constant Schmidt number of 0.5.[4,16]

Thermal and Chemical Nonequilibrium Analysis

The effect of the thermal nonequilibrium of the flow is considered by Park's two-temperature model.[6] We assume that the rotational energy mode is in equilibrium with the translational energy mode at the translational temperature T, and that the vibrational energy modes of all the chemical species are in a Boltzmann distribution at a unique temperature T_V. These assumptions are expected to be valid for the reacting CO_2 gas mixture, since the equilibration of vibrational modes is completed very quickly due to the vibrational-vibrational energy exchanges.[4,17]

The extension and modification of the chemical nonequilibrium viscous shock-layer equations to the thermal and chemical nonequilibrium flow are performed by splitting the energy equation into the translational-rotational energy component and the vibrational energy component in a curvilinear, body-oriented coordinate system.[18] The translational-vibrational energy exchange is basically expressed by the Landau-Teller formula.[6] However, the vibrational relaxation rate is reduced by the diffusive nature of the vibrational relaxation at high temperature and the collision-limiting.[19] As for the diffusive nature of the vibrational relaxation, the modification to the Landau-Teller expression by Wada[19] is employed. According to this modification, the rate of the energy transfer due to the vibrational relaxation for the ith species is expressed as

$$Q_{V,i} = \rho_i \frac{e_{v,i}^{\mathrm{eq}} - e_{v,i}}{\langle \tau_i \rangle} \left[1 - \exp\left(-\frac{\theta_{V,i}}{T_V} \right) \right]^{1.4} \tag{9}$$

The effect of the collision-limiting is taken into account by using the effective relaxation time, which is obtained by blending the T-V relaxation time from Millikan and White, and the average molecular collision time from Park.[6]

The characteristic temperature of the vibrational energy mode for each molecule is obtained from Ref. 14. Carbon dioxide has three vibrational modes, and their characteristic temperatures are 945, 1903, and 3380 K. In the present study, all the vibrational modes of CO_2 are assumed to relax at the slowest relaxation rate, i.e., the rate for the θ_V = 3380 K mode. Camac pointed out that the vibrational relaxation of CO_2 occurs at the rate similar to that of the θ_V = 945 K mode.[17] Camac's rate provides considerably faster relaxation of CO_2 molecules, e.g., about 10 times faster at the temperature of 10,000 K, than the rate determined by the θ_V = 3380 K mode.

In addition to the energy transfer due to the vibrational relaxation, the loss or gain of the vibrational energy due to the dissociation or recombination of molecules should be taken into account in the thermal nonequilibrium analysis. In the present study, it is assumed to be 50% of the dissociation energy of molecules.[6,19]

The chemical reactions considered for the thermal and chemical nonequilibrium analysis are the same as those for the chemical nonequilibrium analysis. It is assumed that the forward dissociation reactions are governed by the rate controlling temperature defined by

$$T_d = \sqrt{T \cdot T_V} \tag{10}$$

in order to consider the effect of the chemical-vibrational coupling.[6] The recombination reactions and the other reactions are assumed to be governed only by the translational temperature.

For the thermal nonequilibrium analysis, we must determine the enthalpy, energy, and specific heat of each species both for the translational-rotational mode and for the vibrational mode. The translational and rotational energy modes are assumed to be fully excited. The enthalpy for each energy mode is expressed as follows[15]:

$$\begin{aligned} h_{tr,i} &= (Cp_{t,i} + Cp_{r,i})(T - T_{\mathrm{ref}}) + h_{0,i} \\ h_{V,i} &= h_i(T_V) - (Cp_{t,i} + Cp_{r,i})(T_V - T_{\mathrm{ref}}) - h_{0,i} \end{aligned} \tag{11}$$

where $h_i(T_V)$ is the enthalpy evaluated at the vibrational temperature from the polynomial curve fit. The energy and specific heat of each mode are computed in the same manner.

Boundary Conditions

In the viscous shock-layer analysis, the computational domain is bounded by the shock wave and body surfaces. The boundary conditions must be specified at these surfaces. The flow just behind the shock wave surface is assumed to be chemically frozen at the freestream compositions. For a thermal nonequilibrium analysis, the vibrational temperature is assumed to be frozen at the freestream temperature. These boundary conditions are determined by the Rankine-Hugoniot relations.

As for the boundary conditions on the body surface, the no-slip condition, the isothermal wall (nominally at 1500 K), and the zero normal gradient at the wall are employed for the velocity, temperature and pressure, respectively. In the

thermal nonequilibrium flow analysis, the vibrational temperature is assumed to be in equilibrium with the translational temperature. This is a good approximation except for the flight regime at fairly high altitudes, where the thermal nonequilibrium is significant, even in the vicinity of the body surface. It is well-known that the wall catalycity augments the wall heating rate significantly. We assess the importance of the wall catalycity by using two extreme cases for the wall catalycity, which are known as NCW and FCW.[3] The NCW condition assumes that the flow is chemically frozen at the wall, and the FCW condition enforces all the gas species to recombine completely to the freestream composition.

Numerical Method

The method of solution is almost the same as presented in Refs. 12 and 13. To keep the numerical stability of the space-marching procedure, the coupling technique,[20] where the normal momentum and the total mass conservation equations are solved in coupled manner, and the under-relaxation technique are employed for the calculations of the pressure and the velocity component normal to the surface. The shock wave shape is determined after four streamwise sweeps. The shock-layer thickness is corrected after every streamwise sweep by considering the balance of the mass flux between the shock wave and the body surface. A 31 × 101 grid is used for the computation of the shock-layer flow over the present vehicle configuration. The grid is clustered in the normal direction both to the shock wave surface and to the body surface in order to capture rapid changes in the nonequilibrium flow properties there. The minimum grid spacing in the normal direction is 5×10^{-4} of the shock standoff distance. The change in the computed heating rate due to further grid refinement up to 2×10^{-4} is within 1% at the perigee altitude. The CPU time required for the single streamwise sweep is about 20 s on the Fujitsu VP-200 at ISAS computer center. The CPU time required for the thermal and chemical nonequilibrium analysis is about 1.2 times of that required for the chemical nonequilibrium analysis.

Results and Discussions

Classification of Flow Chemistry

Figure 1 shows the classification of the stagnation region flow chemistry with respect to the flight velocity and the flight altitude. The flow is considered to be chemically frozen in the flight regime at the velocity below approximately 2.5 km/s, where the temperature behind the shock wave is not high enough to excite the dissociation of carbon dioxide. Then the effects of the thermal and chemical nonequilibrium should be taken into account in the flight regime at the velocity above 2.5 km/s. The solid lines and dashed lines are the contour lines of Δf_δ defined by Eq. (1) for the chemical nonequilibrium and the thermal nonequilibrium, respectively. In the present study, we assume the boundaries for the flight regime of severe chemical nonequilibrium and for that of severe thermal nonequilibrium at the values of Δf_δ 0.1 and 200 K. The chemical nonequilibrium and the thermal nonequilibrium in the shock layer are considered to be significant in the flight regimes above the solid line of the value 0.1, and above the dashed line of the value 200 K, respectively.

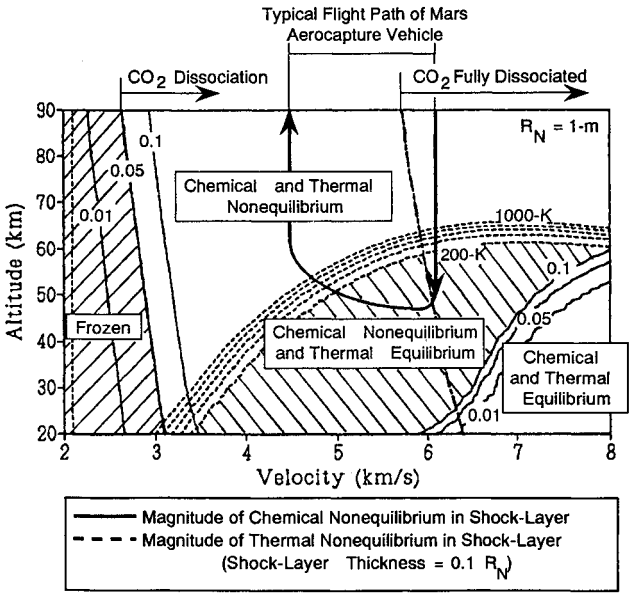

Fig. 1 Classification of stagnation region flow chemistry for Mars aerocapture vehicle.

The typical flight trajectory for a Mars aerocapture vehicle with the entry velocity of 6 km/s is also plotted in Fig. 1. According to this trajectory, the vehicle may always experience severe chemical nonequilibrium effects. The thermal nonequilibrium may be also significant during the atmospheric flight, except the regime around the perigee altitude. When the flight velocity is fixed as 6 km/s, the chemical nonequilibrium effect and the thermal nonequilibrium effect should be taken into account for the analysis of the shock-layer flow at the altitude higher than 25 and 60 km, respectively. In the present method, the flow classification is sensitive to the shock standoff distance as expressed in Eq. (1). When the shock standoff distance is thinner than expected, the boundaries for the chemical and thermal nonequilibrium shown in Fig. 1 will move down to lower altitudes. However, the difference in the flight altitude is less than 10 km, even when the shock standoff distance is reduced from 10 to 5% of the nose radius. It should be noted that this classification is made from a viewpoint of the relaxation of the nonequilibrium quantities, and does not necessarily indicate the significance of the thermal and chemical nonequilibrium of the flow on the wall heating rate.

Such classification as presented in Fig. 1 depends strongly on the thermochemical model of reacting CO_2 and the model of the Martian atmosphere. Figure 2 shows the effect of the vibrational relaxation time of CO_2 on the classification of the stagnation region flow chemistry. As already mentioned, Camac's expression and Millikan and White's expression with θ_V = 945 K yield a considerably faster vibrational relaxation rate than the present model (θ_V = 3380 K). Then by using Camac's rate or the θ_V = 945 K rate in place of the θ_V = 3380 K rate, the boundary line for severe thermal nonequilibrium moves significantly upward on the velocity-altitude diagram at the velocity below 6 km/s. At the velocity above 6 km/s, however, considerable difference among these relaxation models is not observed.

Figure 3 shows the effect of the model of the Martian atmosphere on the classification of the stagnation region flow chemistry. The solid lines and the dashed lines represent the

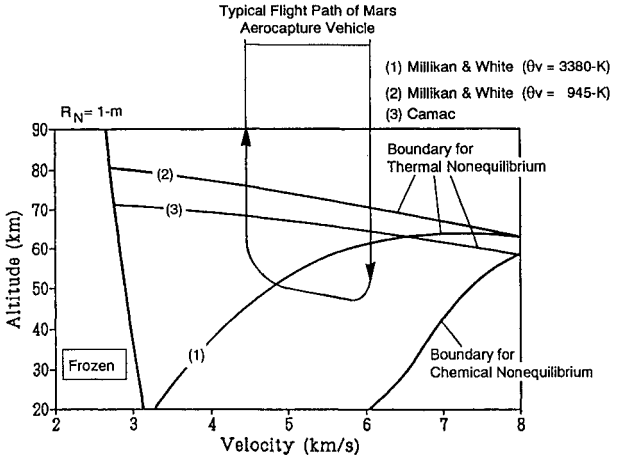

Fig. 2 Effect of vibrational relaxation rate on classification of stagnation region flow chemistry.

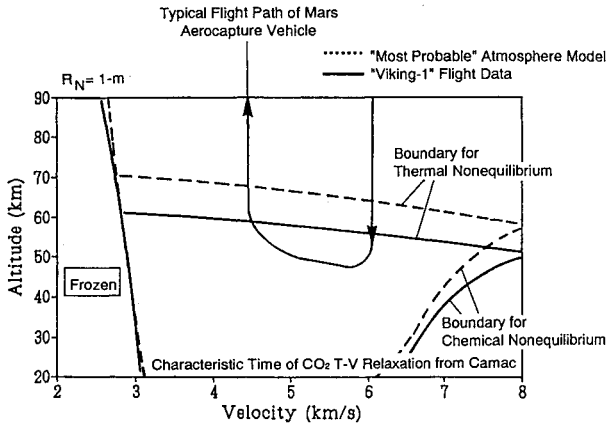

Fig. 3 Effect of Martian atmosphere model on classification of stagnation region flow chemistry.

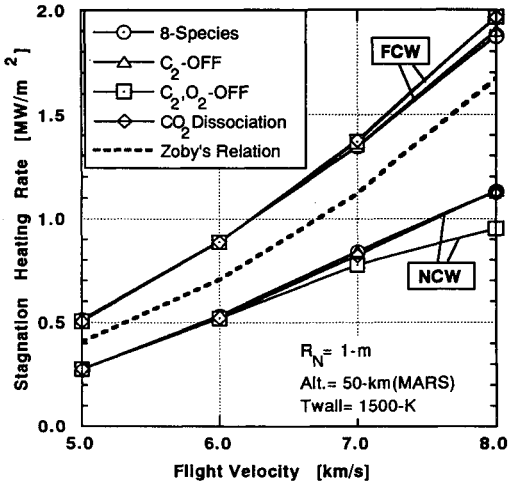

Fig. 4 Sensitivity of stagnation heating rate to chemical reaction model.

boundary lines determined by using the "Viking-1" flight data and the most probable model as the Martian atmosphere model, respectively. In this figure, the vibrational relaxation time is determined by Camac's expression. Since the atmospheric density in the Viking-1 flight data is much smaller than in the most probable model, the boundary line of severe thermal nonequilibrium for the Viking-1 model is located about 10 km below the boundary line for the most probable model. The boundary lines for a frozen chemistry and a severe chemical nonequilibrium effect are not significantly affected by the model of the Martian atmosphere.

Effects of Chemical Nonequilibrium on Wall Heating Rate

The sensitivities of the wall heating rate to the chemical reactions considered in the analysis and the wall temperature are investigated by making the chemical nonequilibrium viscous shock-layer analysis under the assumption of the thermal equilibrium.

In order to assess the importance of the chemical species considered in the chemical nonequilibrium analysis to the wall heating rate, we consider four cases. These are 1) the case with the eight species, 2) the case without C_2, 3) the case without C_2 and O_2, and 4) the case in which only the dissociation of CO_2 is considered. Figure 4 shows the variations of the stagnation wall heating rate with the flight velocity at an altitude 50 km for the above four cases. The importance of each chemical reaction considered in the analysis to the wall heating rate depends on the flight velocity, since the chemical reactions to be excited in the shock layer depend on the temperature behind the shock wave. However, the difference in the wall heating rate due to the choice of the chemical reaction model is negligibly small in comparison with the difference

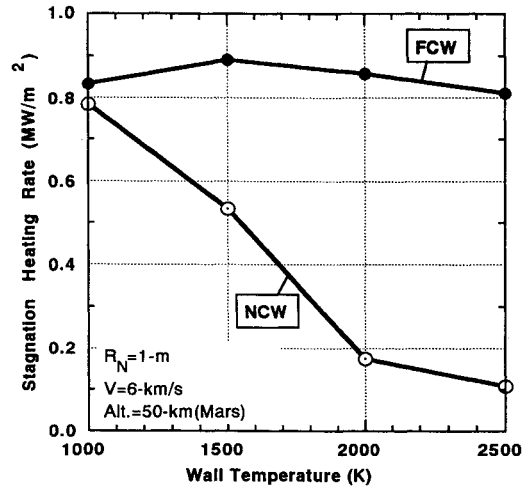

Fig. 5 Variations of stagnation heating rate with wall temperature.

due to the wall catalycity. From a viewpoint of the wall heating rate, the primary reaction in the shock layer is the dissociation of CO_2. In fact, most of the chemical compositions in the shock layer are products of the dissociation reaction of carbon dioxide,[5] since the activation energy for this reaction is quite low in comparison with other dissociation reactions. The results by the empirical relation by Zoby[21] lie between the NCW and FCW results, which may determine the lower and the upper limits of the wall heating rate, respectively. The wall heating rate for the FCW condition is expected to be sensitive to the Schmidt number, since the energy transport to the surface by diffusion exists for this condition. When the Schmidt number is reduced from 0.5 to 0.4, the wall heating rate for the FCW condition increases by about 10%, whereas the wall heating rate for the NCW condition is almost insensitive to the Schmidt number.

In the chemical nonequilibrium flow, the wall heating rate consists of the energy flux due to the thermal conduction and the energy flux transported by the diffusion of the species. The wall heating rate is expected to be affected by the wall temperature, since the energy transport to the wall by the thermal conduction depends on the temperature gradient at the wall. In practice, it is difficult to specify an exact wall temperature, since the wall temperature is governed by the heating rate, the radiative cooling from the surface, and the heat sink capability of the spacecraft body. Figure 5 shows the sensitivity of the stagnation wall heating rate to the wall temperature. The flight velocity and altitude are 6 km/s and 50 km, respectively, and the eight-species model is considered for the chemical reactions of carbon dioxide. For the NCW condition, the energy transport to the wall by the diffusion vanishes, and the wall heating rate decreases significantly with the increase in the wall temperature. On the other hand, the fully catalytic wall is not significantly affected by the wall temperature from a viewpoint of the wall heating rate. In the FCW case, the energy flux to the wall due to the diffusion increases with the increase in the wall temperature, since the dissociation becomes significant in the vicinity of the wall, and the energy release to the flow by the recombination at the body surface due to the wall catalycity increases. The sensitivity of the wall heating rate to the wall temperature strongly depends on the wall catalycity.

Effects of Thermal Nonequilibrium

The effects of the thermal nonequilibrium on the shock-layer thickness, the wall heating rate, and the electron number density in the shock layer are investigated by comparing the results of the thermally and chemically nonequilibrium analysis with those of the thermally equilibrium and chemically nonequilibrium analysis.

The translational and vibrational temperature distributions along the stagnation streamline are shown in Fig. 6. The flight velocity and altitude are 6 km/s and 50 km, respectively. In the thermal nonequilibrium analysis, the difference between the translational temperature and the vibrational temperature seems to vanish asymptotically with the increase in the distance from the shock wave. Then we can determine the characteristic length L for the T-V relaxation by fitting this temperature difference to the expression:

$$\Delta T = \Delta T_{\text{shock}} \exp(-x/L), \qquad \Delta T = T - T_V \qquad (12)$$

In this case, the difference between the thermal equilibrium analysis and thermal nonequilibrium analysis in their temperature profiles appears only at the region near the shock wave. The shock standoff distance for the thermal nonequilibrium case is thicker than that for the thermal equilibrium case. The difference between the thermal equilibrium case and the thermal nonequilibrium case in their flow properties, however, depends on the flight altitude. Figure 7 shows the variations of the characteristic length for the T-V relaxation and the shock standoff distance with the flight altitude. The flight velocity is 6 km/s. When the flight altitude becomes higher than 60 km, the characteristic length for the T-V relaxation and the shock standoff distance increase rapidly,

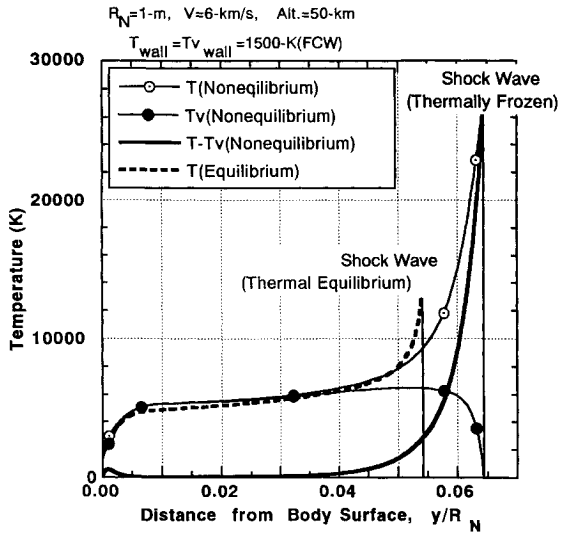

Fig. 6 Translational and vibrational temperature profiles on stagnation streamline.

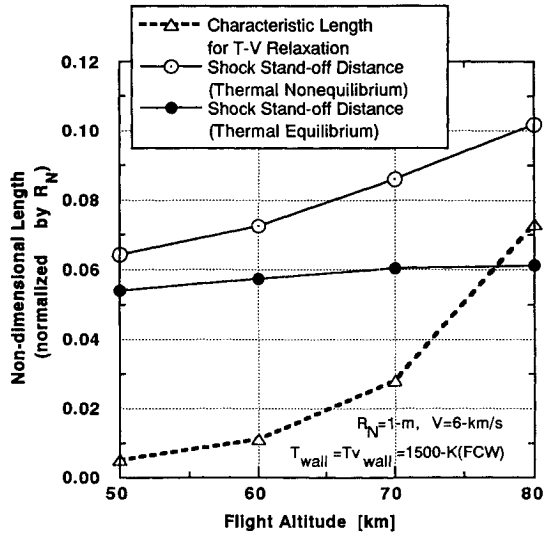

Fig. 7 Variations of shock standoff distance and characteristic length for T-V relaxation with altitude.

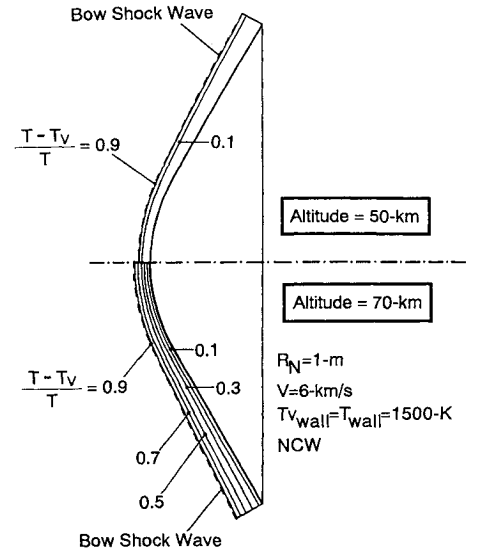

Fig. 8 Extent of thermal nonequilibrium on temperature distribution in shock layer.

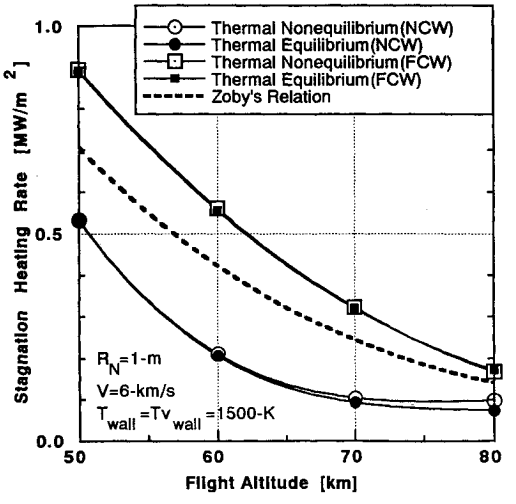

Fig. 9 Effect of thermal nonequilibrium on stagnation heating rate.

whereas in the thermal equilibrium case the shock standoff distance does not increase so significantly. Figure 8 shows the influence of the thermal nonequilibrium on the temperature distribution in the shock layer at altitudes 50 and 70 km. The flight velocity is 6 km/s. Contour lines represent the temperature difference between the translational and vibrational modes, normalized by the local translational temperature. The thermal nonequilibrium region prevails over the shock layer at the altitude 70 km. At the altitude 50 km, the thermal nonequilibrium region is concentrated on the narrow region behind the shock wave, and the shock-layer flow becomes almost thermal equilibrium. Then the classification of the stagnation region flow chemistry in Fig. 1 is appropriate from a viewpoint of the thermal nonequilibrium effect on the temperature distribution in the shock layer.

Figure 9 shows the variation of the stagnation wall heating rate with the flight altitude. The flight velocity is fixed as 6 km/s. The vibrational temperature is assumed to be in equilibrium with the translational temperature on the wall. From a viewpoint of the wall heating rate, the effect of the thermal nonequilibrium is not significant in comparison with the effect of the wall catalycity, except for the slight increase in the wall heating rate under the NCW condition that appears at an altitude above 60 km. Figure 10 shows the distributions of the wall heating rate and its augmentation ratio due to the

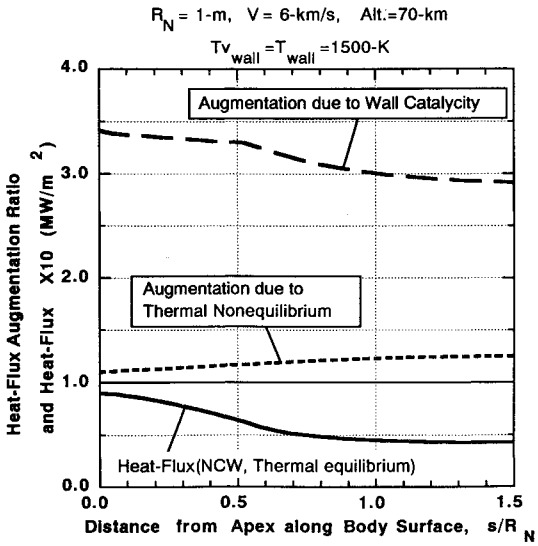

Fig. 10 Wall heating augmentation due to wall catalycity and thermal nonequilibrium along body surface.

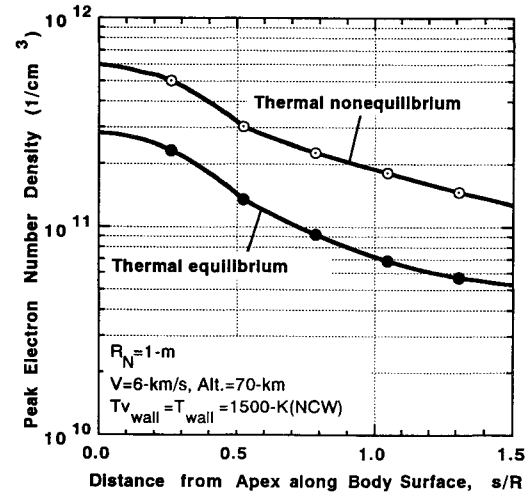

Fig. 11 Distribution of peak electron number density (cm^{-3}) in shock layer along body surface.

thermal nonequilibrium and the wall catalycity along the body surface at an altitude of 70 km. For the present vehicle configuration, the effect of the thermal nonequilibrium on the wall heating rate is also not significant in the downstream region. It should be noted that the actual influences of the thermal nonequilibrium on the wall heating rate and the flow properties in the shock layer are expected to be smaller than predicted in the present analysis, since we assume the slowest relaxation rate for all the vibrational modes of CO_2.

Figure 11 shows the distributions of the peak electron number density along the body surface in the thermal equilibrium and thermal nonequilibrium shock-layer flows. The flight velocity and altitude are 6 km/s and 70 km, respectively. The peak electron number density for the thermal nonequilibrium flow is about twice as high as that for the thermal equilibrium flow both in the stagnation region and in the downstream region, since in the former case, the translational temperature behind the shock wave that governs the ionization rate in the present chemical reaction model is much higher than in the latter case as shown in Fig. 6.

Concluding Remarks

1) The classification of the stagnation region flow chemistry for a Mars aerocapture vehicle is carried out by assuming an asymptotic relaxation process for the thermal and chemical nonequilibrium behind the normal shock wave. It is useful to predict the extent of the flow nonequilibrium in the shock layer in front of a spacecraft.

2) The thermal and chemical nonequilibrium forebody flowfield of a Mars aerocapture vehicle is analyzed numerically by using the viscous shock-layer equations. The shock-layer thickness and the flow properties in the shock layer are affected by the thermal nonequilibrium significantly at altitudes above 60 km. However, the effect of the thermal nonequilibrium on the wall heating rate is not as significant as the effect of the wall catalycity.

3) The sensitivities of the wall heating rate to the uncertainties in the wall condition models are investigated parametrically.

3a) At the Mars aerobraking, the wall catalycity augments the wall heating rate of a spacecraft significantly. Consequently, the chemical nonequilibrium must be taken into account for the prediction of the aerothermodynamic environment around a Mars aerocapture vehicle.

3b) The heat flux to the noncatalytic wall decreases significantly with the increase in the wall temperature, while the heat flux to the fully catalytic wall is hardly affected by the wall temperature.

References

[1]Walberg, G. D., "A Survey of Aeroassisted Orbit Transfer," *Journal of Spacecraft and Rockets*, Vol. 22, No. 1, 1985, pp. 3–18.

[2]Abe, T., Kawaguchi, J., and Suzuki, K., "Feasibility Study of Mars Exploration by Using Aerocapture," *Proceedings of the 1st Workshop on Astrodynamics and Flight Mechanics*, Inst. of Space and Astronautical Science, Kanagawa, Japan, 1991, pp. 1–6.

[3]Suzuki, K., and Abe, T., "Effects of Wall Conditions on Chemically Nonequilibrium Shock-Layer Flow Over Hypersonic Reentry Bodies," *Transactions of the Japan Society for Aeronautical and Space Sciences*, Vol. 36, May 1993, pp. 21–35.

[4]Chen, Y.-K., Henline, W. D., Stewart, D. A., and Candler, G. V., "Navier-Stokes Solutions with Surface Catalysis for Martian Atmospheric Entry," *Journal of Spacecraft and Rockets*, Vol. 30, No. 1, 1993, pp. 32–42.

[5]Suzuki, K., and Abe, T., "Viscous Shock-Layer Analysis of Forebody Flowfield Around Mars Aerocapture Shell," *Proceedings of the 5th Symposium on Computational Fluid Dynamics* (Tokyo, Japan), 1991, pp. 405–408 (in Japanese).

[6]Gnoffo, P. A., Gupta, R. N., and Shinn, J. L., "Conservation Equations and Physical Models for Hypersonic Air Flows in Thermal and Chemical Nonequilibrium," NASA TP-2867, Feb. 1989.

[7]Bobbitt, P. J., "Problems of Atmospheric Entry," NASA SP-258, 1971, pp. 175–288.

[8]Seiff, A., and Kirk, D. B., "Structure of Atmosphere of Mars in Summer at Mid-Latitudes," *Journal of Geophysical Research*, Vol. 82, Sept. 1977, pp. 4364–4378.

[9]Suzuki, K., and Abe, T., "Viscous Shock-Layer Analysis on Thermally and Chemically Nonequilibrium Forebody Flow of Mars Aerocapture Vehicle," AIAA Paper 93-2839, July 1993.

[10]Blottner, F. G., "Prediction of Electron Density in the Boundary Layer on Entry Vehicles with Ablation," NASA SP-252, 1971, pp. 219–240.

[11]Gupta, R. N., Lee, K. P., Moss, J. N., and Sutton, K., "Viscous Shock Layer Analysis of the Martian Aerothermal Environment," *Journal of Spacecraft and Rockets*, Vol. 29, No. 5, 1992, pp. 633–640.

[12]Moss, J. N., "Reacting Viscous-Shock-Layer Solutions with Multicomponent Diffusion and Mass Injection," NASA TR R-411, June 1974.

[13]Miner, E. W., and Lewis, C. H., "Hypersonic Ionizing Air Viscous Shock-Layer Flows over Nonanalytic Blunt Bodies," NASA CR-2550, May 1975.

[14]Allison, D. O., "Calculation of Thermodynamic Properties of Arbitrary Gas Mixtures with Modified Vibrational-Rotational Corrections," NASA TN D-3538, Aug. 1966.

[15]Gupta, R. N., Yos, J. M., and Thompson, R. A., "A Review of Reaction Rates and Thermodynamic and Transport Properties for the 11-Species Air Model for Chemical and Thermal Nonequilibrium Calculations to 30000 K," NASA TM 101528, Feb. 1989.

[16]Candler, G. V., and MacCormack, R. W., "The Computation of Hypersonic Ionized Flows in Chemical and Thermal Nonequilibrium," AIAA Paper 88-0511, Jan. 1988.

[17]Candler, G. V., "Computation of Thermo-Chemical Nonequilibrium Martian Atmospheric Entry Flows," AIAA Paper 90-1695, June 1990.

[18]Sakamura, Y., and Nishida, M., "Numerical Calculation of Thermal and Chemical Nonequilibrium Flows Around a Hypersonic Reentry Vehicle," *Transactions of the Japan Society for Aeronautical and Space Sciences*, Vol. 34, May 1991, pp. 27–45.

[19]Wada, Y., Ogawa, S., Kubota, H., and Akimoto, T., "On the Thermo-Chemical Models for Hypersonic Flows," *Proceedings of the 4th International Symposium on Computational Fluid Dynamics*, Univ. of California, Davis, Davis, CA, 1991, pp. 1173–1178.

[20]Waskiewicz, J. D., Murray, A. L., and Lewis, C. H., "Hypersonic Viscous Shock-Layer Flow over a Highly Cooled Sphere," *AIAA Journal*, Vol. 16, No. 2, 1978, pp. 189–192.

[21]Zoby, E. V., "Empirical Stagnation-Point Heat-Transfer Relation in Several Gas Mixtures at High Enthalpy Levels," NASA TN D-4799, Oct. 1968.